Biosensors and Bioelectronics 96 (2017) 351–357

Contents lists available at ScienceDirect

Biosensors and Bioelectronics

journal homepage: www.elsevier.com/locate/bios

Sensitive sulfide ion detection by optofluidic catalytic laser using horseradish peroxidase (HRP) enzyme

Chaoyang Gong[a], Yuan Gong[a,b,c,*], Maung Kyaw Khaing Oo[b], Yu Wu[a,c], Yunjiang Rao[a], Xiaotian Tan[b], Xudong Fan[b,**]

[a] Key Laboratory of Optical Fiber Sensing and Communications (Ministry of Education of China), University of Electronic Science and Technology of China, Chengdu, Sichuan 611731, China
[b] Department of Biomedical Engineering, University of Michigan, Ann Arbor, MI 48109, USA
[c] Center for Information in BioMedicine, University of Electronic Science and Technology of China, Chengdu 611731, China

ARTICLE INFO

Keywords:
Sulfide ion detection
Optofluidic laser
Catalytic reaction
Horseradish peroxidase (HRP) enzyme

ABSTRACT

We report an optofluidic catalytic laser for sensitive sulfide ion detection. In the catalytic reaction, horseradish peroxidase (HRP) enzyme is used for catalyzing the non-fluorescent substrate, 10-Acetyl-3,7-dihydroxyphenoxazine (ADHP), to produce highly fluorescent resorufin, which was used as gain medium for lasing. Using sulfide ions as inhibitors, the catalytic reaction slows down, resulting in a delay in the lasing onset time, which is used as the sensing signal. The sensing mechanism of the catalytic laser is theoretically analyzed and the performance is experimentally characterized. Sulfide anion is chosen as a model ion because of its broad adverse impacts on both environment and human health. Due to the optical feedback provided by the laser, the small difference in the sulfide ion concentration can be amplified. Consequently, a detection limit of 10 nM is achieved with a dynamic range as large as three orders of magnitude, representing significant improvement over the traditional fluorescence and colorimetric methods. This work will open a door to a new catalytic-laser-based chemical sensing platform for detecting a wide range of species that could inhibit the catalytic reaction.

1. Introduction

Ions play unique and vital roles at different scales, ranging from cell biochemistry (Brown et al., 1993) to ocean acidification (Orr et al., 2005). Optical methods are one of the mainstream technologies for ion concentration detection. Traditionally, the fluorescent and colorimetric mechanisms are used. The former relies on the quenching (Barati et al., 2016; Tang et al., 2013; Wang et al., 2013) or recovery (Gore et al., 2013; Sun et al., 2016; Wang et al., 2015; Z.X. Wang et al., 2014) of fluorescence, whereas the latter uses the absorption of light (Chen et al., 2015; Hatamie et al., 2014; Zhang et al., 2011). Since these technologies inherently do not have high sensitivity, novel nanomaterials such as nanoparticles (Hatamie et al., 2014; Zhang et al., 2011), nanowires (H. Wang et al., 2014), nanosheets (Wang et al., 2016), nanoclusters (Gao et al., 2016; Wang et al., 2015; Z.X. Wang et al., 2014; Xu et al., 2016), and quantum dots (Gore et al., 2013), are being explored to improve the sensitivity. The drawbacks of complex synthesis process, fluctuations in uniformity, tendency to aggregate, limit the potential of nanomaterials-based ion sensors. Here, as an alternate option, we develop an optofluidic catalytic laser for sensitive ion detection.

Optofluidic lasers has been extensively investigated for sensitive intra-cavity biochemical analysis (Fan and Yun, 2014; Humar and Yun, 2015; Sun and Fan, 2012; Wu et al., 2014). In comparison with the traditional fluorescence and colorimetric based detection, the optical feedback mechanism of laser is able to amplify small changes in the gain medium, thus achieving high sensitivity (Fan and Yun, 2014; Wu et al., 2014). Here, we explore the possibility to combine the optofluidic laser technology and enzyme catalytic reaction inside a laser cavity for the detection of ion concentration. The fluorescent product generated by the enzyme-substrate reaction is used as the gain medium. The concentration of the product increases over the reaction time. When the gain reaches a concentration threshold, the laser emission starts to emerge. However, in the presence of ions, which act as an inhibitor, the catalysis process slows down. Consequently, it takes longer time for laser emission to occur. The delay in the laser onset time can thus be used as the sensing signal. In this work, we theoretically analyze the sensing mechanism of the catalytic laser and experimentally character-

* Correspondence to: No. 2006, Xiyuan Ave., High-Tech Zone (West), Chengdu, Sichuan 611731, China.
** Correspondence to: 1101 Beal Ave., Ann Arbor, MI 48109, USA.
E-mail addresses: ygong@uestc.edu.cn (Y. Gong), xsfan@umich.edu (X. Fan).

http://dx.doi.org/10.1016/j.bios.2017.05.024
Received 8 March 2017; Received in revised form 6 May 2017; Accepted 11 May 2017
Available online 12 May 2017
0956-5663/

Table 1
Comparison of different methods for sulfide ion detection.

Technology platform	Sensing principle	Detection limit (μM)	Dynamic range (μM)	Dynamic range, 10Log (C_{max}/C_{min})[a]	References
Fluorescence	Quenching and recovery	0.18	0.5–5	10.0	Wang et al. (2013)
		1.35	1.35–10	8.7	Tang et al. (2013)
		0.28	0.5–8	12	
		0.88	0.88–25	14.5	H. Wang et al., 2014
		0.32	2–10	7	Barati et al. (2016)
	Quenching	50	50–1000	13	Xu et al. (2016)
		0.42	0.5–12	13.8	Wang et al. (2016)
		0.2	0.2–12	17.8	Gao et al. (2016)
		1.1	5–100	13	Sun et al. (2016)
		6.5	3.1–56.2	12.6	Gore et al. (2013)
		0.31	0.31–700	33.5	Z.X. Wang et al., 2014
		0.38	0.5–80	22	Wang et al. (2015)
	Enzyme inhibition	1.0	1.0–10	10	This work
Colorimetric	Absorbance by UV–vis	0.28	0.5–15	14.8	Chen et al. (2015)
	spectroscopy	8.1	12.5–50	6	Hatamie et al. (2014)
		0.3	0.3–10	15.2	Zhang et al. (2011)
	Plasmonic wavelength shift	0.5	0.5–5	10	Huang et al. (2014)
Phosphorescence	Quenching	0.138	2.67–596	23.5	Zhou et al. (2010)
Resonance Rayleigh scattering	Conformation changes	0.24	0.81–308.4	25.8	Yan et al. (2016)
Amperometric	Enzyme inhibition	0.3	1.1–16.3	11.7	Savizi et al. (2012)
Optofluidic laser	Enzyme inhibition	0.01	0.01–10	30	This work

[a] C_{max} and C_{min} are the maximum and minimum detectable concentrations of S^{2-}.

ize the laser performance. Sulfide anion (S^{2-}) is chosen as a model ion due to its wide negative impacts in both environment and healthcare (Bagarinao, 1992; Yang et al., 2009). A detection limit of 10 nM is achieved with a dynamic range of three orders of magnitude, which represents a significant improvement over the state-of-the-art (see Table 1 for comparison). The results agree well with the theoretical analysis. Potential improvement in the sensing performance is also discussed.

2. Theoretical analysis

As illustrated in Fig. 1, the enzyme catalytic reaction occurs when the enzyme, the substrate and hydrogen peroxide (H_2O_2) are mixed, which converts the transparent substrate into the highly fluorescent product that is used as the gain medium. The product concentration increases with the reaction time. Laser emission can be observed under a fixed optical pump when the product concentration reaches a threshold for lasing. In the presence of inhibitors such as S^{2-}, the enzyme activity is suppressed at first (Fig. 1b) due to the binding of inhibitors to the enzyme-substrate complex. Then S^{2-} is consumed and oxidized by H_2O_2, leading to the recovery of the enzyme activity and the catalytic reaction rate. A higher S^{2-} concentration results in a longer recovery time and hence a longer laser onset time, which can be used as the sensing mechanism for inhibitor detection.

We develop a theoretical model to analyze ion detection mechanism based on the optofluidic catalytic laser described above. The laser emission can be expressed as (Wu et al., 2014)

$$I_{Laser}(t) = I_0 \cdot \left[W_{pump} \left(\frac{[P]}{\gamma [C]_0} - 1 \right) - 1 \right], \quad (1)$$

where I_0 is a constant, W_{pump} is the pump intensity, $[P]$ is the concentration of the fluorescent product. $[C]_0$ is the initial concentration of the substrate. γ is the fraction of the product molecules in the excited state at the lasing threshold. Note that γ remains constant for a given optofluidic laser.

According to the laser theory, once the pump intensity exceeds the threshold intensity, i.e., $W_{pump} \geq W_{th}$, laser emission emerges. In our experiment, by using a fixed W_{pump}, the laser threshold can be represented by the threshold concentration of the product (Wu et al., 2014)

$$[P]_{th} = [C]_0(\gamma / W_{pump} + \gamma). \quad (2)$$

As the concentration of product increases with reaction time, the threshold concentration can be further converted to the threshold time, named laser onset time in this work. The temporal changes of $[P]$ can be calculated by

$$[P](t) = \int_0^t v(t)dt, \quad (3)$$

where $v(t)$ is the reaction rate of the enzyme catalytic reaction, which, according to the Michaelis–Menten theory, is given by Cornish-Bowden (1974)

$$v(t) = \frac{V_{max}[C]}{K_m + (1 + [S]/k_i)[C]}, \quad (4)$$

where K_m is the Michaelis-Menten constant. $[C] = [C]_0 - [P]$ is the substrate concentration after certain reaction time. $V_{max} = k_{cat} \cdot [E]_0$ denotes the maximum reaction rate. k_{cat} is the turnover number, i.e., the maximum number of substrate molecules converted to product per enzyme molecule per second. $[E]_0$ is the enzyme concentration. $[S]/k_i$ is an inhibition term, with $[S]$ the concentration of inhibitor S^{2-} and k_i the inhibition constant.

In the mixture, S^{2-} is oxidized by H_2O_2. The decreasing of $[S]$ can be described by the rate equation (Millero et al., 1989)

$$\frac{d[S]}{dt} = -k \cdot [S] \cdot [H_2O_2], \quad (5)$$

where k is the rate constant. $[H_2O_2]$ is the concentration of H_2O_2, given by

$$[H_2O_2] = [H_2O_2]_0 - ([S]_0 - [S]) = \Delta + [S], \quad (6)$$

where $\Delta = [H_2O_2]_0 - [S]_0$ is the initial concentration difference between H_2O_2 and S^{2-}. By solving Eqs. (5) and (6), we arrive at

$$[S] = \frac{\Delta}{\beta e^{\Delta kt} - 1}, \quad (7)$$

where $\beta = [H_2O_2]_0/[S]_0$.

In the Supplementary material, simulation results based on the theory are given. Fig. S1 shows temporal changes of the S^{2-} concentration. It decreases exponentially with time. The calculated reaction rate as a function of time is shown in Fig. S2 under different initial S^{2-}

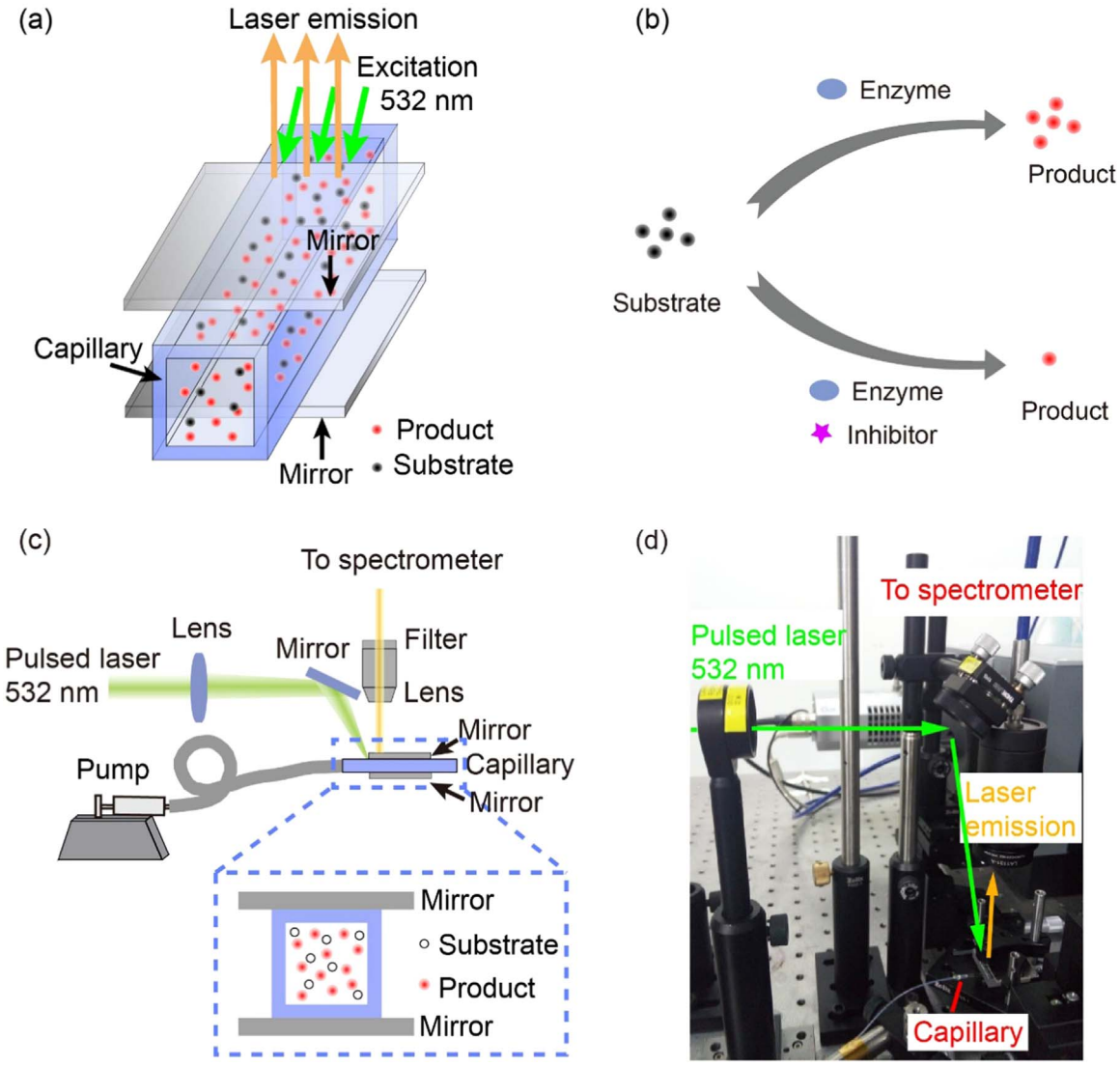

Fig. 1. (a) Structure of the laser cavity for the optofluidic catalytic laser. (b) Generation of the product as gain material and effect of the inhibitor on the catalytic reaction. (c) Schematic and (d) a photo of the experimental setup.

concentrations, $[S]_0$. In the absence of S^{2-}, the normalized reaction rate remains nearly unity, indicative of an uninhibited reaction. The slight decrease of the reaction rate is due to the consumption of substrate. In the presence of S^{2-}, the initial rate is nearly zero, suggesting that the enzyme activity is significantly inhibited at the beginning. When the S^{2-} concentration continues to decrease due to the oxidization by H_2O_2, the rate increases with time. Eventually, when the S^{2-} concentration approaches zero, the reaction reaches the maximal rate and the enzyme activity is completely recovered. Apparently, more time is needed for the enzyme to recover its activity at a higher inhibitor concentration. The laser intensity, according to Eq. (1), is calculated and shown in Fig. S3. The laser intensity curves show longer delays in the laser onset time with increasing S^{2-} concentration and the same laser output rate above the lasing threshold, indicating the enzyme activity recovers completely after the onset time.

3. Material and methods

3.1. Experimental setup

Experimental setup of the optofluidic laser is illustrated in Fig. 1. A silica capillary (Friedrich & Dimmock Inc.) with an inner square cross section of 1.0 mm × 1.0 mm and a wall thickness of 0.5 mm was used as the microfluidic channel. It was sandwiched between two highly reflective dielectric mirrors, which formed a Fabry-Perot (FP) laser cavity. The reflectivities of the upper and bottom mirrors were 91.5% and 99.5%, respectively. Reagents were flowed through the capillary and the enzyme catalytic reaction occurred in bulk solution, rather than on surface, in the capillary. A 532 nm pulsed laser (Continuum, 5 ns pulse width, 20 Hz repetition rate) was used as pump and focused on the capillary from the edge of the upper mirror. Laser emission or fluorescence was collected by a lens and sent to a spectrometer (Andor, SR-500I-A). In order to maximize the laser detection efficiency and minimize the fluorescence background, we used a 1 mm diameter aperture to spatially filter out the fluorescence background and collect predominantly the directional laser emission.

3.2. Materials

Enzyme has been extensively used in biochemistry due to its ability to amplify a weak signal (Andersen et al., 1993). We chose enzyme horseradish peroxidase (HRP) in our experiment due to its high efficiency and stability. A salt-free lyophilized HRP powder (No. 31490) was purchased from Thermo Fisher. HRP stock solution of 2 mg/ml was prepared by dissolving the HRP powder in 0.1 M potassium phosphate buffer (pH 6.0) at room temperature. Then the

HRP working solution with a concentration of 20 ng/ml was freshly prepared using 10-fold serial dilutions by the same buffer. An enhanced chemifluorescent HRP substrate kit (No. 15159) was also purchased from Thermo Fisher. It contains 10-Acetyl-3,7-dihydroxyphenox-azine (ADHP) concentrate, enhancer, and stable peroxide solution. ADHP is a well-documented, non-fluorescent substrate that can be catalyzed by HRP to produce resorufin, a highly fluorescent product.

S^{2-} is an effective inhibitor for HRP (Yang et al., 2004). A 200 mM S^{2-} stock solution was prepared daily by dissolving sodium sulfide ($Na_2S{\cdot}9H_2O$) in deionized (DI) water. $Na_2S{\cdot}9H_2O$ (No. S101399) was purchased from Aladdin BioChem Co. The S^{2-} working solutions were prepared using 10-fold serial dilutions in DI water and freshly used right after preparation. In order to quantitatively investigate the influence of the H_2O_2 concentration on S^{2-} sensing, H_2O_2 (No. H112515, Aladdin BioChem), instead of H_2O_2 in the substrate kit (as the manufacturer does not provide its concentration), was used. The optimal H_2O_2 working solution was prepared by diluting H_2O_2 stock solution (10 M) with DI water by 40,000 times dilution, i.e., 250 μM. The substrate working solution was prepared by mixing 100 μl of optimal H_2O_2 solution, 100 μl of enhancer and 2 μl of ADHP concentrate, as suggested by Thermo Fisher.

For S^{2-} sensing, 10 μl of S^{2-} solution was mixed with 90 μl of working HRP (20 ng/ml) and then mixed with the substrate working solution at a volume ratio of 1:19. The resultant final concentration of HRP was 0.9 ng/ml. The final mixture was injected into the capillary and the emission spectra was recorded over time at a steady condition. The reagent preparation processes and the regeneration of the microfluidic channel after each test are described in supplementary materials.

4. Results and discussion

4.1. Detection method and experimental optimization

The effect of the H_2O_2 concentration on the reaction was firstly investigated by the fluorescent detection with the S^{2-} concentration fixed at 10 μM. The spectrally integrated intensity of the fluorescence was plotted as a function of reaction time with different H_2O_2 concentrations (Fig. 2a). The reaction had three stages, which was reflected by the temporal evolution of the fluorescent output (e.g., green dots, Fig. 2a). Between $t = 0$ and $t = t_1$, H_2O_2 reacted mainly with free S^{2-} ions so that the enzyme activity remained completely suppressed and there was no fluorescence emission. Between $t = t_1$ and $t = t_2$, H_2O_2 continued to oxidize the S^{2-} ions, leading to gradual enzyme activity recovery. Consequently, a gradual increase in the fluorescent intensity can be observed. Finally, the slope of the fluorescent intensity versus time reached a constant value at t_2, indicating that all S^{2-} ions were depleted and the enzyme activity was fully recovered. The slope decreased as the concentrations of H_2O_2 decreased, reveals that the enzyme activity was recovered more slowly at lower H_2O_2 concentration.

We introduce the equivalent onset time (τ_f) for fluorescence, defined as the reaction time at which the integrated intensity reaches a value of 5×10^4. The onset time difference is calculated by $\Delta\tau_f = \tau_f - \tau_{0,f}$ with τ_f and $\tau_{0,f}$ the onset times in the presence and absence of S^{2-}, respectively. The onset time difference decreased with an increasing H_2O_2 concentration (Fig. 2b).

The H_2O_2 concentration was optimized by considering two factors. First, the concentration of H_2O_2 should be high enough to achieve a complete recovery of enzyme activity. In Fig. 2a, the slopes for 125 μM and 62.5 μM of H_2O_2 were evidently smaller than that of the higher concentrations, indicating that the enzyme activity was not fully recovered. Similarly, in the laser experiments, we were unable to achieve lasing with 125 μM and 62.5 μM of H_2O_2, which also reflected the fact that enzyme activity was not fully recovered. Second, high concentration of H_2O_2 was not desirable for detecting low concentrations of inhibitors. Fig. 2b shows that the higher the H_2O_2 concentration, the shorter the laser or fluorescence onset time, making it difficult to distinguish the onset time difference between two low concentrations of inhibitors. Based on the trade-off between the above two factors, we chose the optimal H_2O_2 concentration to be 250 μM, which, as shown later, would result in an excellent S^{2-} sensitivity with a relatively large dynamic range. By using Fig. 2b as a calibration curve, the optofluidic catalytic laser can also be used for H_2O_2 sensing, which is important for many biochemical applications such as immunoassays (De La Rica and Stevens, 2012).

4.2. S^{2-} sensing by fluorescence detection

The fluorescence spectra at different reaction time with or without inhibitor are compared in Figs. 3a and b. In the absence of S^{2-}, the catalytic reaction occurred and fluorescent product of resorufin was generated immediately after mixing HRP with the substrate. As the reaction continued, the product concentration, hence the fluorescence intensity, increased with time. In the presence of S^{2-}, the catalytic reaction slowed down due to the inhibition of HRP. The spectrally integrated intensity at different S^{2-} concentration was calculated and plotted in Fig. 3c. The onset time difference was calculated by $\Delta\tau_f = \tau_f - \tau_{0,f}$ with τ_f and $\tau_{0,f}$ the onset times in the presence and absence of S^{2-}, respectively. As shown in Fig. 3d, the onset time difference was indistinguishable when S^{2-} concentrations below 1 μM.

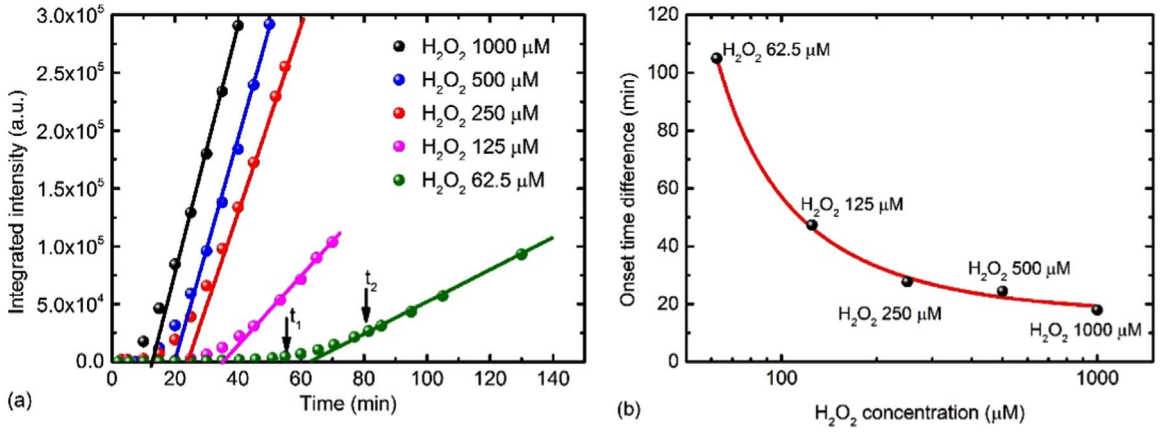

Fig. 2. (a) Spectrally integrated intensity of fluorescence as a function of reaction time at different H_2O_2 concentrations. The intensity was spectrally integrated between 560 nm and 700 nm. (b) Fluorescence equivalent onset time difference as a function of H_2O_2 concentration in the semi-logarithmic scale. (For interpretation of the references to color in this figure, the reader is referred to the web version of this article.).

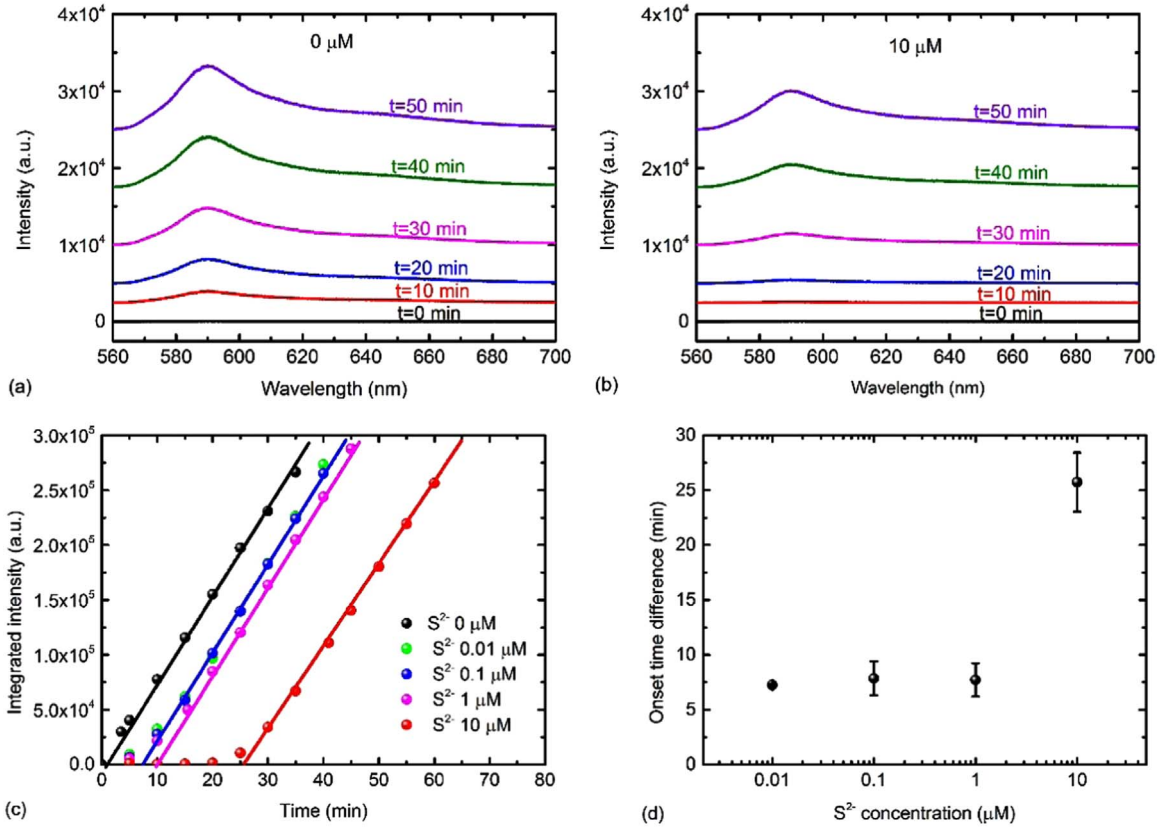

Fig. 3. Fluorescence spectra at different reaction times (a) in the absence of S^{2-} and (b) with 10 μM S^{2-}. (c) Spectrally integrated intensity as a function of reaction time with different S^{2-} concentrations. The intensity was spectrally integrated between 560 nm and 700 nm. (d) Fluorescence onset time difference as a function of S^{2-} concentration, with the logarithmic scale in the x-axis and the linear scale in the y-axis. Error bars were obtained based on triplicate measurements.

4.3. Characterization of optofluidic laser

The optofluidic laser experiment was performed by sandwiching the capillary between two mirrors to provide the optical feedback. We firstly used the saturated fluorescent product as gain medium, by mixing 100 ng/ml of HRP with the substrate working solution at a volume ratio of 1:19 and incubated for 30 min Fig. 4 shows the integrated intensity as a function of pump energy density, showing a laser threshold of about 3.8 μJ/mm^2, which is two orders of magnitude lower than the previous optofluidic laser (Wu et al., 2014), due to the significant improvement in mirrors' reflectivities (~140 times lower in transmission loss). The inset shows the emission spectrum of the optofluidic catalytic laser.

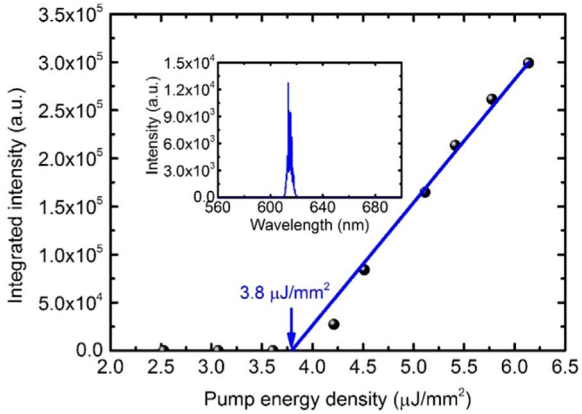

Fig. 4. The spectrally integrated intensity as a function of pump energy density. The intensity was integrated between 610 nm and 625 nm. Inset, the laser spectrum of the optofluidic catalytic laser at a pump energy density of 4.2 μJ/mm^2.

4.4. S^{2-} sensing by optofluidic laser

The laser spectra at different reaction times with or without inhibitor are compared in Figs. 5a and b. The pump energy density was fixed at 180.5 μJ/mm^2. S^{2-} as an inhibitor delayed the laser onset time. In the absence of S^{2-}, the laser emission started to emerge at ~80 min, after which the laser intensity grew quickly and saturated in 10 min. With 10 μM S^{2-}, the laser emission appeared at ~160 min. There was an onset time difference of ~ 80 min between 0 and 10 μM of S^{2-}.

The spectrally integrated intensity was plotted as a function of the reaction time (Fig. 5c). Once the lasing occurred, the intensity grew much more quickly than the corresponding growth of the fluorescence in Fig. 3c, because of the strong nonlinear nature of the lasing process near the threshold. The sharp transition is one of the advantages for the optofluidic laser to determine the onset time with higher accuracy than that by the fluorescence-based detection. The laser onset time can be considered as a temporal threshold at which the gain concentration reached a threshold for lasing. The laser onset time increases with an increasing S^{2-} concentration. Once the lasing is achieved, the slopes of the laser intensity above the threshold are nearly identical, suggesting that the enzyme activity was fully recovered and the effective enzyme concentration remained the same for all these measurements. In contrast, the previous studies (Wu et al., 2014) showed that the different enzyme concentrations would result in different slopes of the integrated intensity versus time.

Fig. 5d shows the laser onset time difference as a function of the S^{2-} concentration. Similar to the fluorescence-based detection discussed previously, the laser onset time difference, $\Delta\tau$, is used as the sensing signal. $\Delta\tau = \tau - \tau_0$, where τ and τ_0 are the laser onset time in the presence and absence of S^{2-}, respectively. Here, the laser onset time is defined as the time when the integrated intensity reaches 5.0×10^4 in

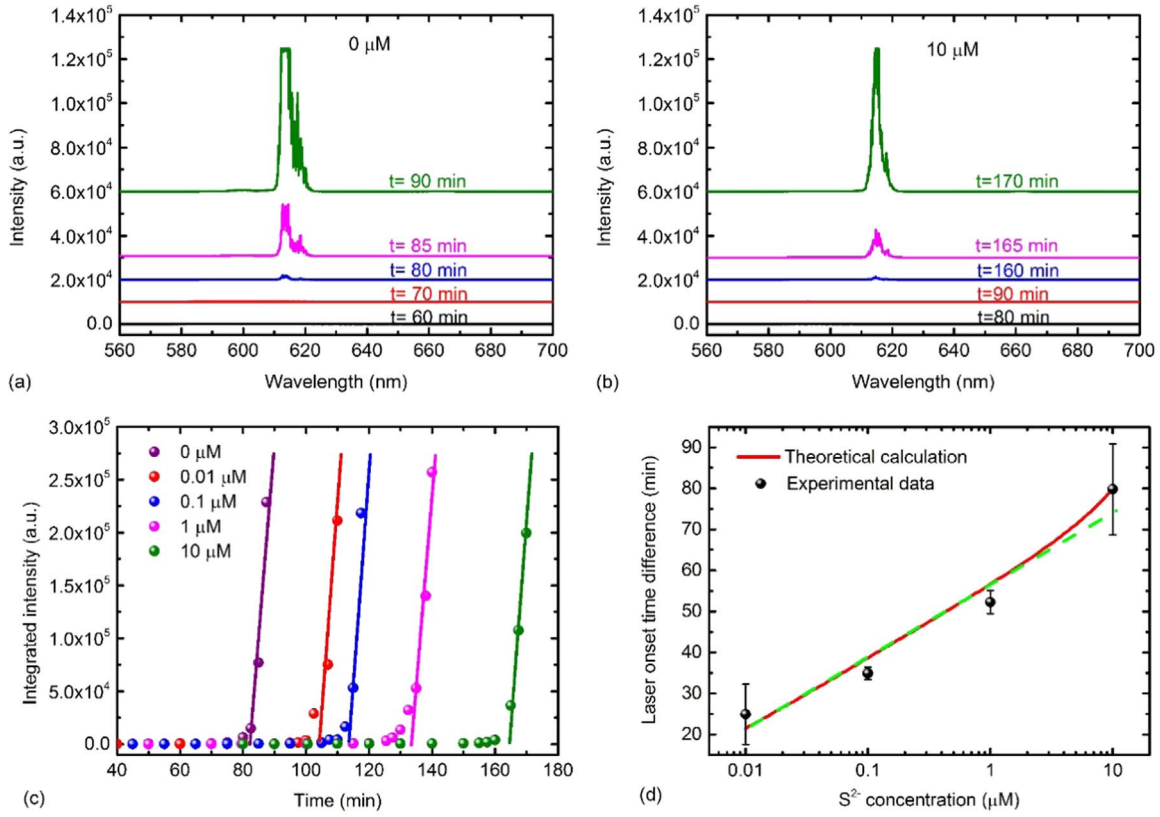

Fig. 5. Emission spectra evolution of the optofluidic catalytic laser (a) in the absence of S^{2-} and (b) with 10 μM S^{2-}. Curves are vertically shifted for clarify. (c) Spectrally integrated intensity as a function of reaction time with different S^{2-} concentrations. The solid lines are the linear fits of data above the threshold time. The intensity was spectrally integrated between 610 nm and 625 nm. (d) Laser onset time difference versus S^{2-} concentration. Error bar was calculated based on triplicate measurements. The solid red curve is the theoretical simulation and the green dashed line is a linear extension. (For interpretation of the references to color in this figure legend, the reader is referred to the web version of this article.)

Fig. 5c. Such choice of the laser onset time is somewhat arbitrary. However, it will not affect the quantitation of the ion concentration, as what matters is the onset time difference in the presence and absence of ions. The optofluidic catalytic laser showed a high sensing performance, with a lower LOD of 10 nM and an upper LOD of 10 μM, corresponding to a dynamic range of three orders of magnitude. Detailed comparison with other technologies for S^{2-} sensing is given in Table 1, showing that the optofluidic laser is highly competitive in terms of sensitivity and dynamic range. The significantly improved sensing performance over the fluorescence-based method (Fig. 3) is due mainly to the lasing effect, which amplifies the slight ion concentration difference that cannot be distinguished by fluorescence.

The experimental result is in good agreement with the theoretical prediction (Fig. 5d). The green dashed line is a linear extension from the simulated data in the range of 0.01 μM to 1 μM. The experimental deviation from the linear trend at 10 μM S^{2-} can be accounted for by the consumption of H_2O_2 at a high S^{2-} concentration, which slightly slows down the catalytic reaction rate.

Now we discuss the strategies to further improve the laser based ion detection. The lower LOD of S^{2-} is mainly determined by the minimal number of S^{2-} ions needed to inhibit one enzyme molecule. In our experiment, the enzyme concentration was 0.9 ng/ml (~0.02 nM). The lower LOD of 10 nM corresponds to 500 S^{2-} ions per enzyme molecule, which agrees roughly with the ratio of molecular weights (MW) of HRP (MW = 44,000 Da) and S^{2-} (MW=32 Da). To improve the lower LOD, lower H_2O_2 concentration should be helpful if the Q-factor of the laser cavity is high enough to get the lasing emission.

There are several methods to further enhance the upper LOD. First, a higher H_2O_2 concentration is preferred for oxidizing more S^{2-} and recovering the enzyme activity. Second, high Q factor microcavities can be used as the laser resonator to achieve a lower threshold concentration of the product and a shorter laser onset time for higher concentration of S^{2-}. Third, more stable HRP can be used so that the enzyme catalytic reaction can be sustained at a longer time in order to measure higher S^{2-} concentrations. The enzyme activity of HRP degrades with time and the lyophilized HRP powder is not as good as the HRP solution in the ELISA kits (DY206 from R & D Systems). In addition, the dual-mode strategy, by using both laser and fluorescence detections, can be employed to further extend the dynamic range (Wu et al., 2014).

We experimentally confirmed that the laser onset time can be shortened by utilizing higher HRP enzyme concentration or higher pump energy density. By increasing the enzyme concentration from 0.5 ng/ml to 4 ng/ml with a fixed pump energy density of 180.5 μJ/mm^2, the onset time decreased from 21.8 min down to 1.7 min (Fig. S4a). By increasing the pump energy density from 60.1 μJ/mm^2 to 240.7 μJ/mm^2 with a fixed enzyme concentration of 1 ng/ml, the onset time decreased from 11.2 min down to 6.5 min (Fig. S4b). In both cases, the H_2O_2 in the substrate kits were used, which also contributed to the acceleration of the lasing process.

5. Conclusion

We have developed an optofluidic catalytic laser platform for sensitive sulfide ion detection with a large dynamic range. A theoretical model has also been developed reveal the operation of the optofluidic catalytic laser and the sensing principle. The catalytic reaction between the HRP enzyme and ADHP substrate has been used to produce the gain medium for lasing. The optofluidic laser takes advantage of the intrinsic amplification mechanism and uniquely employs the lasing onset time as the sensing signal. Our work will provide a new route for chemical sensing by using optofluidic catalytic lasers. It also provides a

method to modulate the laser via chemical reaction, which is useful in developing novel functional photonic devices in the future.

Acknowledgement

We acknowledge the financial support from the National Natural Science Foundation of China (61575039), Fundamental Research Funds for the Central Universities (ZYGX2015J137), the 111 Project (B14039), and the National Science Foundation (DBI-1451127).

Appendix A. Supporting information

Supplementary data associated with this article can be found in the online version at doi:10.1016/j.bios.2017.05.024.

References

Andersen, L., Dinesen, B.O., Jørgensen, P.N., Poulsen, F., Røder, M.E., 1993. Clin. Chem. 39, 578–582.
Bagarinao, T., 1992. Aquat. Toxicol. 24, 21–62.
Barati, A., Shamsipur, M., Abdollahi, H., 2016. Sens. Actuators B 230, 289–297.
Brown, E.M., Gamba, G., Riccardi, D., Lombardi, M., Butters, R., Kifor, O., Sun, A., Hediger, M.A., Lytton, J., Hebert, S.C., 1993. Nature 366, 575–580.
Chen, C., Zhao, D., Lu, L., Yang, F., Yang, X., 2015. Sens. Actuators B 220, 1247–1253.
Cornish-Bowden, A., 1974. Biochem. J. 137, 143–144.
De La Rica, R., Stevens, M.M., 2012. Nat. Nanotechnol. 7, 821–824.
Fan, X., Yun, S.H., 2014. Nat. Methods 11, 141–147.
Gao, Z., Liu, F., Hu, R., Zhao, M., Shao, N., 2016. RSC Adv. 6, 66233–66241.
Gore, A.H., Vatre, S.B., Anbhule, P.V., Han, S.H., Patil, S.R., Kolekar, G.B., 2013. Analyst 138, 1329–1333.
Hatamie, A., Zargar, B., Jalali, A., 2014. Talanta 121, 234–238.
Huang, H., Li, Q., Wang, J., Li, Z., Yu, X.F., Chu, P.K., 2014. Plasmonics 9, 11–16.
Humar, M., Yun, S.H., 2015. Nat. Photonics 9, 572–576.
Millero, F.J., LeFerriere, A., Fernandez, M., Hubinger, S., Hershey, J.P., 1989. Environ. Sci. Technol. 23, 209–213.
Orr, J.C., Fabry, V.J., Aumont, O., Bopp, L., Doney, S.C., Feely, R.A., Gnanadesikan, A., Gruber, N., Ishida, A., Joos, F., Key, R.M., Lindsay, K., Maier-Reimer, E., Matear, R., Monfray, P., Mouchet, A., Najjar, R.G., Plattner, G., Rodgers, K.B., Sabine, C.L., Sarmiento, J.L., Schlitzer, R., Slater, R.D., Totterdell, I.J., Weirig, M., Yamanaka, Y., Yool, A., 2005. Nature 437, 681–686.
Savizi, S.P., Kariminia, H.R., Ghadiri, M., Roosta-Azad, R., 2012. Biosens. Bioelectron. 35, 297–301.
Sun, H., Lu, D., Xian, M., Dong, C., Shuang, S., 2016. Anal. Methods 8, 4328–4333.
Sun, Y., Fan, X., 2012. Angew. Chem. Int. Ed. 51, 1236–1239.
Tang, L., Cai, M., Huang, Z., Zhong, K., Hou, S., Bian, Y., Nandhakumar, R., 2013. Sens. Actuators B 185, 188–194.
Wang, H., Mu, L., Jin, L., She, G., Xu, H., Shi, W., 2014. RSC Adv. 4, 60086–60091.
Wang, J., Long, L., Xie, D., Zhan, Y., 2013. J. Lumin. 139, 40–46.
Wang, L., Chen, G., Zeng, G., Liang, J., Dong, H., Yan, M., Li, Z., Guo, Z., Tao, W., Peng, L., 2015. New J. Chem. 39, 9306–9312.
Wang, Y., Hu, J., Zhuang, Q., Ni, Y., 2016. ACS Sustain. Chem. Eng. 4, 2535–2541.
Wang, Z.X., Zheng, C.L., Ding, S.N., 2014. RSC Adv. 4, 9825–9829.
Wu, X., Oo, M.K.K., Reddy, K., Chen, Q., Sun, Y., Fan, X., 2014. Nat. Commun. 5, 3779.
Xu, N., Li, H.W., Yue, Y., Wu, Y., 2016. Nanotechnology 27, 425602.
Yan, S., Song, R., Tang, Y., 2016. Anal. Methods 8, 3768–3773.
Yang, X.F., Wang, L., Xu, H., Zhao, M., 2009. Anal. Chim. Acta 631, 91–95.
Yang, Y., Yang, M., Wang, H., Jiang, J., Shen, G., Yu, R., 2004. Sens. Actuators B 102, 162–168.
Zhang, J., Xu, X., Yuan, Y., Yang, C., Yang, X., 2011. ACS Appl. Mater. Interfaces 3, 2928–2931.
Zhou, T., Wang, N., Li, C., Yuan, H., Xiao, D., 2010. Anal. Chem. 82, 1705–1711.